ISSN: 2689-1204

Research Article

Journal of Applied Material Science & Engineering Research

Investigation of Marangoni Convective Flow of Hybrid Nanofluids in Darcy-Forchheimer Porous Medium

Hamid Qureshi[1], Sehrish Rani[2] and Sebastian Andreas Altmeyer[3*]

[1]*Department of Mathematics, Mohi-Ud-Din Islamic University, Pakistan*

[2]*Govt. Graduate College, Asghar Mall, Pakistan*

[3]*Universitat Politecnica de Catalunya, EETAC `School of Telecom and Aerospace Engineering, Spain*

***Corresponding Author**
Sebastian Andreas Altmeyer, Universitat Politecnica de Catalunya, EETAC `School of Telecom and Aerospace Engineering, Spain.

Submitted: 2024, Sep 28; **Accepted:** 2024, Oct 24; **Published:** 2024, Nov 27

Citation: Qureshi, H., Rani, S., Altmeyer, S. A. (2024). Investigation of Marangoni Convective Flow of Hybrid Nanofluids in Darcy- Forchheimer Porous Medium. *J App Mat Sci & Engg Res, 8*(4), 01-14.

Abstract

In this study we performed a comprehensive numerical investigation of the Marangoni convective flow through a Darcy-Forchheimer porous matrix in nanofluids and their hybrid equivalents - hybrid nanofluids. Convection occurred predominantly at the liquid-air interface within the porous structure. The governing equations were numerically solved using a finite difference approach, Python was used to obtain the solutions of the differential equations. In this paper, we discuss different important key parameters that qualitatively and quantitatively impact flow and heat transfer properties, respectively. We focused on the effects of porosity and thermocapillarity. The present investigation studied the Marangoni convection in (hybrid) nanofluids of manganese zinc ferrite (MnZnFe2O4) and nickel zinc ferrite (NiZnFe2O4) with water (H2O) as a base fluid. Furthermore, the effects of the parameters involved in the Darcy- Forchheimer model on the convective flow, temperature and concentration characteristics are discussed and analyzed methodically. We elucidate the specific results and awareness of areas to improve in thermal management systems, providing useful information with a high potential for the future development of applications in engineering disciplines crucially impacted by heat transfer performance.

Keywords: Hybrid Nanofluids, Darcy-Forchheimer, Marangoni Convective Flow, Thermocapillarity, Heat Transfer

1. Introduction

There is significant research interest in nanofluids (NFs) from a theoretical, fundamental and industrial perspective. The elevated thermal characteristics of these types of fluids are essential for engineering applications. This interest has rapidly increased in recent years due to the combination of different nanofluids with hybrid nanofluids (HNFs). Marangoni convection is prominent among all the transport phenomena governing the motion of advanced, complex fluids and their thermal properties and could noticeably influence the process where the surface tension becomes responsive to temperature or concentration gradients [1]. Thermal transport analysis of nanofluids has received significant attention due to the importance of the effective cooling of electronic equipment. The main focus has been the analysis of the buoyant motion and thermal dissipation of nanofluids due to their promising prospects in enhancing heat transport [2-6]. Kashyap and Das numerically investigated the entropy production generated by the thermal transport of a nanofluid-filled porous domain subjected to different nonuniform boundary conditions[7]. Nevertheless, the quantitative and numerical studies on Marangoni convective flow in nanofluids and hybrid-nanofluids are limited, especially regarding Darcy-Forchheimer matrix porous media.

This work aimed to fill this gap in the research. To the best of our knowledge this study presents the first Python-based comparative numerical investigation of the Marangoni convective flow in nanofluids and their hybrid systems in a Darcy-Forchheimer porous channel. This research is necessary to enhance heat transfer efficiency and learn about the complex flow dynamics in advanced fluids. Therefore, this research important in developing the best industrial processes involving cooling, filtration, and energy systems to ensure efficiency better designs. Moreover, it offers basic scientific insight and will help develop predictive models for various engineering applications. The flow details, heat transfer and concentration in a given system modeled using non-linear mathematics and numerical simulations. The thermocapillary force and porosity were considered for the equations. We utilized Python aided computational methods while considering the conducive flow

characteristics and heat transfer rates. The numerical solutions of the governing equations were obtained by applying the solve-bvp algorithm and importing the SciPy, NumPy and Matplotlib environments.

This research focused on the Marangoni convection in NiZnFe2O4 and MnZnFe2O4 Nano-solutes with water H2O as the base liquid. We believe that this work offers new insights and meaningful numeric data via the detailed examination of the influences of different parameters in the combined Darcy-Forchheimer model on convective flow, temperature and concentration fields [8]. This research may enhance optimum thermal control configurations and foster the advancement of engineering disciplines in which heat transfer plays a significant role.

The high potential for industrial engineering applications is key motivation for this increasing interest. Heat convection and heat transfer across extended surfaces have crucial practical importance in engineering and industry including glass paper manufacturing, radioactive wastes, case involving chemical reactions that produce heat energy that is absorbed into a system, and blood rheology. The continuously increasing interest in nanofluids especially regarding thermal conductivity, has resulted in works on this topic, which are predicted to grow [9]. It is impossible to name them all here, but we intend to provide an overview of relevant works in this study. Buongiorno analyzed the heat transfer of a micropolar nanofluid above a permeable stretchable/flexible boundary layer and found that it can either contract or expand [10]. Many other works have provided key studies concerning heat conduction, entropy production, the slip behavior in the steady stagnation point flow of different types of nanofluids, and the magneto hydrodynamics (MHD) flow of NFs and HNFs [11-13]. In addition, the peristalsis-like movement of HNFs, entropy optimization, and dusty fluids, which include several particles have been studied [14,15].

Moreover, the heat transfer in convective MHD flow in an elliptic permeable skin involving hybrid-nanofluid has been of particular interest [16-18]. Alsabery et al. investigated MHD flow with the convective boundary of a low polarity liquid at the microscopic level over an extending surface[19]. Other works have presented a new Casson fluid model and discussed the Jeffery fluid flow over a porous extending surface [20-22]. Hayat et al. discussed the flow of carbon nanotubes (CNTs) with thermal conductivity in entropy generation with a surface curvature over an expanding arc [23]. From a theoretical perspective studying and understanding the influence of Arrhenius activation energy in a non-Newtonian Nano liquid with MHD radiative and Brownian movement flow is particular interesting [24,25].

Additionally, Hayat et al. described the Ree-Eyring non-Newtonian Nano liquid flow between spinning disks with entropy optimization and the effects of the activation energy on those Nano liquids [26]. Ijaz et al. analyzed the physical effects of Joule heating and chemical reactions on Walter-B Nano liquid and discussed the heat exchange without a mechanical connection [27].

Several works have studied the entropy generation in non-Newtonian liquids under the influence of a magnetic field [28-31]. S. Qayyum et al. carried out theoretical research on the MHD flow of a parabolic shaped surface. Recent developments in the field have considered nanofluids embedded in porous media [32]. The result of torrential and numerical works regarding chemical reactions within Darcy- Forchheimer flow through a porous matrix have indicated the great potential of this setup [33-35]. Khan et al. discussed the second order velocity slip flow scenario of a colloidal fluid dispersed in a base fluid based on, which Shafiq et al. examined the impacts of the slip condition and the Arrhenius activation energy on the flow of a rotating nanofluid [36,37].

Surface or Marangoni convection signifies the combination of heat and mass transfer processes that occur in the higher-pressure regions within a fluid and here transferred to the low-pressure regions within the same fluid [1]. The importance lies in the movements of the near-surface convection flow in nanofluids as observed in different works [38-40]. Later works discussed some stochastic computational findings concerning with NFs and HNFs [41-43].

This article used numerical analysis to provides information about nanofluids (NFs) and their hybrid counterparts (HNFs) composed of both nanoparticles alongside a comprehensive comparison of both types of fluids. This could be useful for researchers working in the thermal management domain. A diagram of the various applications of such thermal hybrid nanofluids (THNFs) is illustrated in Figure 1. We advanced the study of Marangoni convective flows in multi-phase, complex porous structures using the noval and latest computational environment of the Python advanced numerical solver algorithm (Solve-bvp), which will benefit current and future work in this field.

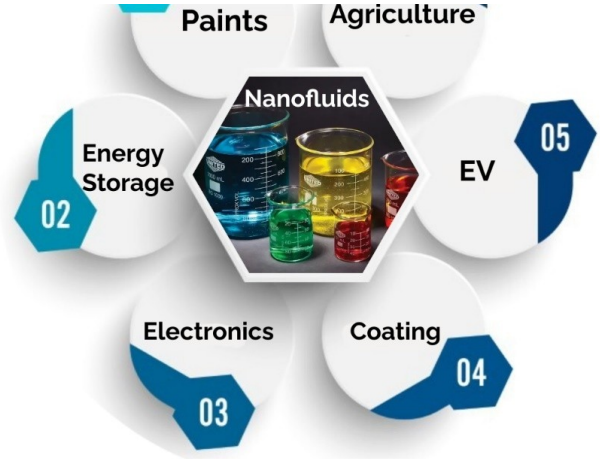

Figure 1: Applications of Thermal Hybrid Nanofluids (THNFs)

2. Materials and Methods

In this study, we considered the incompressible, steady hybrid nanofluid flow of $MnZnFe_2O_4$ and $NiZnFe_2O_4$ with water as the base fluid to gain inside into the heat and mass transfer at the higher vs lower pressure surface areas within hybrid nanofluids. Additional effects such as entropy generation, viscous dissipation, and the effect of Darcy-Forchheimer porous media were incorporated. The equations modeled based on the previously mentioned assumptions were as follows [41];

$$\frac{\partial u}{\partial x}+\frac{\partial v}{\partial y}=0 \tag{1}$$

$$u\left(\frac{\partial u}{\partial x}\right)+v\left(\frac{\partial v}{\partial y}\right)+\frac{\upsilon_{HNF}}{P^*}+F\,u^2=\left(\frac{\mu_{HNF}}{\rho_{HNF}}\right)\left(\frac{\partial u^2}{\partial y^2}\right) \tag{2}$$

$$u\left(\frac{\partial T}{\partial x}\right)+v\left(\frac{\partial C}{\partial y}\right)-\frac{k_{HNF}}{(\rho C_p)_{HNF}}\frac{\partial^2 T}{\partial y^2}=\left(\frac{\mu_{HNF}}{(\rho C_p)_{HNF}}\right)\left(\frac{\partial u}{\partial y}\right)^2 \tag{3}$$

$$u\left(\frac{\partial C}{\partial x}\right)+v\left(\frac{\partial C}{\partial y}\right)+k_0^2(C-C_\infty)\left(\frac{T}{T_\infty}\right)^n e^{-E_a/KT}=D\left(\frac{\partial^2 C}{\partial y^2}\right) \tag{4}$$

$$\mu_{HNF}\left(\frac{\partial u}{\partial y}\right)=\left(\frac{\partial \sigma}{\partial x}\right)=\sigma_0\left(\gamma_c\left(\frac{\partial C}{\partial x}\right)_{y=0}+\gamma_T\left(\frac{\partial T}{\partial x}\right)_{y=0}\right) \tag{5}$$

with the following boundary conditions

$$v=0, T-T_\infty=T_0 X^2 \text{ when } y=0, \tag{6}$$

$$u=0, T-T_\infty=0, C-C_\infty=0, \text{ if } y\to\infty \tag{7}$$

$$\sigma=\sigma_0\left(1-\gamma_T(T-T_\infty)-\gamma_C(C-C_\infty)\right) \tag{8}$$

$$\gamma_T=\frac{-1}{\sigma_0}\frac{\partial \sigma}{\partial T} \text{ at } T=\infty \text{ and } \gamma_C=\frac{-1}{\sigma_0}\frac{\partial \sigma}{\partial C} \text{ at } C=\infty \tag{9}$$

These equations address the continuity (Eq. 1), momentum (Eq. 2), energy (Eq. 3), concentration (Eq. 4), and surface tension gradient (Eq. 5). Impermeable surface and infinity boundary conditions (Eq. 6-8) were assigned with temperature and concentration dependencies (Eqs. 8-9) for the fluid behavior at the surface.

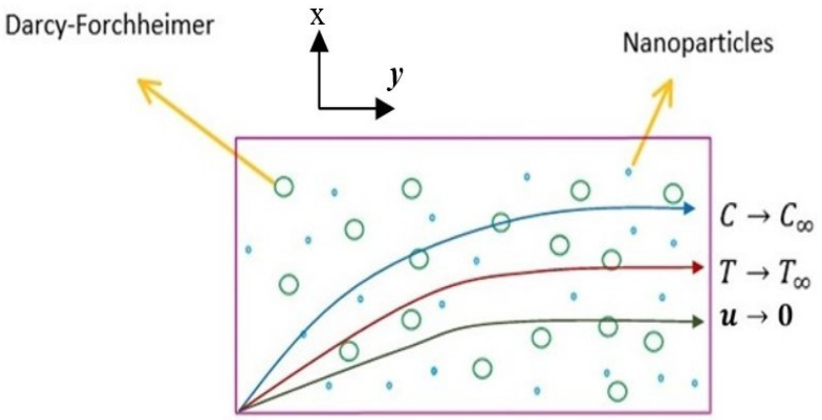

Figure 2: Spatial Structure of Geometry

For $y \to \infty$, the flow regularities of the hybrid nanofluid demonstrates that the flow velocity u=0, which means that it gives an impression that as one is far away from the source of the boundary conditions, the effects of the boundary layer is almost insignificant. At the same time, the temperature difference $T - T_\infty$ and the concentration difference $C - C_\infty$ decrease and go to zero, consequently, temperature and concentration of nanofluid approach to the values of T_∞ and C_∞, respectively. Such behavioral patterns show that the distal reactions are extinguished to the state of the system and therefore the heat and mass transfer become negligibly insignificant. The asymptotic behavior of the present hybrid nanofluid and consequences of this phenomenon offers insights into the long-run efficiency of this technology.

The geometric structure of the extending surface is shown in Figure 2, describing the boundary constraints for the momentum, temperature, and concentration. C_∞ and T_∞ represent the concentration and temperature away from the sheet surface, respectively. C_w and T_w denote the concentration and temperature on the surface boundary, respectively. The surface is porous, like stone or ground soil. These pores are connected and significantly affect the flow. Petroleum engineering, ground-water flow, and chemical engineering are major users of such a model.

Material	ρ (kg / m^3)	C $_p$ (J / kg K)	k (W /m K)
$H\,2O$	997.1	4179	0.613
MnZnFe2 o4	4700	1050	3.9
NiZn$Fe2\ o4$	4800	710	6.3

Table 1: Thermal Properties and Characteristics of NF and HNF [44].

The y-axis is horizontal, and the x-axis is vertical. The convection occurs along the y-axis, following a convenient natural flow direction. γ_s and γ_c are the temperature and concentration constants. is the Boltzmann number, the surface tension is represented by σ, and the activation energy is presented by E_a. T_0 and T_∞, and C_0 and C , represent the reference and ambient temperature and concentrations, respectively. $(\rho C_p)_{HNF}$ and k_{HNF} denote the heat capacitance and thermal conductivity of the hybrid nanofluid. C_p is the specific heat capacity. The chemical reaction rate is k_1, and the permeability of the porous medium is P^*. The mass diffusivity is symbolized with D, the dynamic viscosity is denoted by μ_{HNF}, and the density is denoted by ρ (x, y) are the axis coordinates.

The following similarity variables were introduced to transform the governing equations into a dimensionless form:

$$u=\frac{v_f}{L}Xf'(\eta), v=\frac{v_f}{L}f(\eta), \eta=\frac{y}{L}, X=\frac{x}{L}, \theta(\eta)=\frac{T-T_\infty}{T_0X^2}, \phi(\eta)=\frac{C-C_\infty}{C_0X^2} \quad (10)$$

Equation (1) is satisfied insignificantly by the relations in (10), as higher-order terms are neglected; thus, the solution may deviate from the original value by a minute difference in the region of higher- order flow. Eqs. (2-4) were converted into the following forms:

$$f'''(\eta)=(1-\sigma_1)^{2.5}(1-\sigma_2)^{2.5}A_1\left((f')^2-ff''+F_r(f')^2\right)+f' \quad (11)$$

$$\theta''(\eta)=\frac{A_2 Pr}{A_3}\left(2\theta' f-\theta f'\frac{E_c(f')^2}{(1-\sigma_1)^{2.5}(1-\sigma_2)^{2.5}A_2}\right) \tag{12}$$

$$\phi'(\eta)=Sc\left(k_1(\delta\theta+1)^n\exp\left(\frac{-E_1}{\delta\theta+1}\right)\psi(\eta)+2\phi f'-\phi' f\right) \tag{13}$$

Using Eq. (10), Eqs. (6) and (7) took the following form to synchronize with Eq. (11)–(13). The boundary conditions given in (6 - 9) thus became

$$f=0, f'=-2(1+r)(1-\sigma_1)^{2.5}(1-\sigma_2)^{2.5}, \theta=1, \phi=1, \eta=0$$
$$f'=0, \theta=0, \phi=0 \text{ when } \eta\to\infty. \tag{14}$$

The thermal properties and characteristics of the NF and HNF [39] are presented in Table 1. Moreover, the pre-eminent parameters involved in Eqs. (11)–(13) and the boundary conditions in (14) are listed in Table 2.

The dimensionless Skin Friction and Nusselt numbers [45] are,

$$C_{fx}\sqrt{Re}=\frac{f''(0)}{\left((1-\sigma_1)(1-\sigma_2)\right)^{2.5}} \text{ and } \frac{Nu_x}{\sqrt{R}}=\frac{k_{HNF}}{k_{NF}}\theta'(0) \tag{15}$$

The relations of the *Entropy* and *Bejan numbers* [43] in dimensionless form are,

$$N_G=A_3\delta\theta'^2+\frac{BrRe}{\left((1-\sigma_1)(1-\sigma_2)\right)^{2.5}}f''^2+L\frac{\delta_1\phi'^2}{\delta} \tag{16}$$

$$Be=\frac{A_3\delta\theta'^2+L\theta'+L\frac{\delta_1\phi'^2}{\delta}}{N_G}, \tag{17}$$

where

$$A_1=\frac{\rho_{HNF}}{\rho_f}=(1-\sigma_2)\left((1-\sigma_1)+\sigma_1\frac{\rho_{S1}}{\rho_f}\right)+\sigma_2\frac{\rho_{S2}}{\rho_f} \tag{18}$$

$$A_2=\frac{(\rho c_p)_{HNF}}{(\rho c_p)_f}=(1-\sigma_2)\left((1-\sigma_1)+\sigma_1\frac{(\rho c_p)_{S1}}{(\rho c_p)_f}\right)+\sigma_2\frac{(\rho c_p)_{S2}}{(\rho c_p)_f} \tag{19}$$

$$A_3=\frac{k_{HNF}}{k_f} \tag{20}$$

$$\frac{k_{HNF}}{k_f}=\frac{k_{S2}-2\sigma_2(k_{NF}-k_{S2})+2k_{NF}}{k_{S2}+\sigma_2(k_{NF}-k_{S2})+2k_{NF}} \tag{21}$$

$$\frac{k_{NF}}{k_f}=\frac{k_{S1}-2\sigma_1(k_f-k_{S1})+2k_f}{k_{S1}+\sigma_1(k_f-k_{S1})+2k_f} \tag{22}$$

$$\frac{\mu_{HNF}}{\mu_f}=\frac{1}{\left((1-\sigma_1)(1-\sigma_2)\right)^{2.5}} \tag{23}$$

An empirical correlation was used to express the effective viscosity of the mono and hybrid nanofluids as a function of the volume fraction and interaction between the two different types of nanoparticles. The mono and hybrid nanofluids, with regard to their thermal properties, were computed using the Maxwell–Garnett models for their effective thermal conductivity.

The most significant parameters and their formulas are listed in

Table 2. We considered the following parameters:

• The inverse Darcy coefficient [45], related to heat loss due to friction;

• The Marangoni number indicating how crucial or significant surface tension forces are compared with viscous forces [46];

• The Darcy number denoted as P^* / l^2, where k is the permeability, and l is the characteristic length [47];

• The Forchheimer number (Fr) explaining the reasons for obtaining the nonlinear drag consequences in the porous media [48];

• The Reynolds number (Re) determining whether the flow of a fluid is smooth or turbulent [49];

• The Prandtl number (Pr) the C1 momentum diffusivity divided by the thermal diffusivity[50];

• The Nusselt number (Nu) describing the conduction of heat across the surface [51].

These parameters characterize the fluid flow, heat transfer, porosity effects, nonlinear drag, and hybrid nanofluid parameters and are the principal parameters underlining the forces and transport processes. The inverse Darcy coefficient, B, measures the resistance to the flow of a fluid through porous structures; the permeability is its reciprocal value. Schmidt's parameter links the rates of momentum and mass diffusion in fluids, which might be connected to mass transfer problems. k1 is the chemical reaction rate, which is generally temperature-dependent. Ea is the activation energy, namely, the energy a reaction needs. The temperature coefficient δ is frequently applied in material sciences to express alterations in physical properties with temperature variations. Br, the Brinkmann number, compares the viscous and inertial forces in fluid flow, similar to the Reynolds number. L is the diffusion constant, which indicates the ease with which substances spread in a material. The Eckert ratio, Ec, is the ratio of kinetic energy to enthalpy and is important in high-velocity flows. The concentration coefficient δ1 measures a substance's rate of passage through a phase proportional to the variation in physical properties with the concentration. These are all key parameters (Table 2) used in various fields, including fluid dynamics, heat transfer, mass transport, and chemical reactions, to describe and analyze different physical phenomena.

Parameter	Relation
Inverse Darcy coefficient	$B=\left(\frac{\nu_f}{\alpha_f}\right)\frac{L^2}{K}$
Forchheimer parameter	$Fr=\frac{C_b}{\sqrt{K}}$
Prandtl ratio	$Pr=\frac{\nu_f}{\alpha_f}$
Schmidt parameter	$Sc=\frac{\nu_f}{D_f}$
Chemical reaction rate	$k_1=\frac{k_0 L^2}{\nu_f}$
Activation energy coefficient	$E=\frac{E_a}{kT_\infty}$
Temperature coefficient	$\delta=\frac{T_0 X^2}{T_\infty}$
Brinkmann parameter	$Br=\frac{\mu v_f^2}{kT_0 L^2 X^2}$
Diffusion constant	$L=\frac{R * DC_0}{k_f}$

Eckert ratio	$Ec=\frac{v_f^2}{c_p T_0 L^2 X^2}$
Concentration coefficient	$\delta_1=\frac{C_0 X^2}{C_\infty}$
Marangoni parameter	$r=\frac{\gamma_c C_0}{\gamma_T T_0}$

Table 2: Thermophysical Parameters and Formulas [44]

3. Solution Methodology

The governing equations were solved using the advanced Python bvp-solver, using the mean variability in the description of the solution. This provided a fused setting for computing nonlinear PDEs while creating a new fluid flow model to enhance the HNF's capability in a Darcy–Forchheimer medium operating in a porous phase. First, the set of expressions with splines made up for the addressed group of transforms with the exactification of the fine-tuning parameters. Subsequently, the obtained set of ODEs was used to generate numerical solutions employing the Python computational environment and systematically incorporating the finite difference algorithm for the velocity, temperature, and concentration of the HNF ($Mn\ Zn\ Fe_2O_4 + Ni\ Zn\ Fe_2O_4 + H_2O$) and NF ($Mn\ Zn\ Fe_2O_4 + H_2O$).

The Python code, which solved the boundary value problem using `solve_bvp`, took a mesh of 100 equidistant nodes between the bounds 0 and 3 to obtain a balance between computational efficiency and accuracy. A mesh independence study needed to be carried out to ensure the solution's robustness. This could be achieved by running different mesh sizes, e.g., 50, 100, and 200 nodes, and checking whether refining the mesh size generated stable results. Furthermore, it needed to provide a detailed sensitivity analysis of the key parameters and how they might influence the solution—e.g., thermal conductivity and porosity factors—while estimating the numerical error to ensure the approach's accuracy.

This study described the flow velocities, temperature fluctuations, and concentration changes and considered eight key principal parameters. The corresponding values of the three analyses for each parameter are provided to investigate the effects of the changes in both caloric and momentum at the modified wall boundaries.

The parametric integrated values for the model's computational procedure are presented in Table 3, and other extensive variables and coefficients have been omitted based on this assumption. The chosen parameters based on their properties relevant to the thermocapillary characteristic were as follows:

- Porous media effects (Darcy-Forchheimer)
- Surface tension forces (Marangoni)
- Nonlinear drag effects (Forchheimer)
- Thermal and momentum transport (Eckert and Prandtl)
- Mass transport and diffusion (Schmidt)
- Chemical reactions and activation energy
- Reaction kinetics (chemical reaction rate)

The variations in these parameters were aligned with the analysis of their individual and combined impacts on the temperature, momentum, and mass transport in the HNF and NF. The coefficients, like the Reynolds and Nusselt numbers, were not varied as they were related to the flow regime and buoyancy.

Scenarios	Cases	Parameters							
		B	***r***	***Fr***	***Ec***	***Pr***	***Sc***	***E***	***k1***
S-1 B for $f'(\eta)$ profile	1	**0.2**	0.3	0.2	0.2	2.0	0.8	0.2	0.2
	2	**0.6**	0.3	0.2	0.2	2.0	0.8	0.2	0.2
	3	**1.0**	0.3	0.2	0.2	2.0	0.8	0.2	0.2
S-2 r for $f'(\eta)$ profile	1	0.3	**0.2**	0.2	0.2	2.0	0.8	0.2	0.2
	2	0.3	**0.6**	0.2	0.2	2.0	0.8	0.2	0.2
	3	0.3	**1.0**	0.2	0.2	2.0	0.8	0.2	0.2

S-3 *Fr* for $f'(\eta)$ profile	1	0.3	0.2	**0.2**	0.2	2.0	0.8	0.2	0.2
	2	0.3	0.2	**0.6**	0.2	2.0	0.8	0.2	0.2
	3	0.3	0.2	**1.0**	0.2	2.0	0.8	0.2	0.2
S-4 *Ec* for θ(*η*) profile	1	0.3	0.2	0.2	**0.0**	2.0	0.8	0.2	0.2
	2	0.3	0.2	0.2	**0.5**	2.0	0.8	0.2	0.2
	3	0.3	0.2	0.2	**1.0**	2.0	0.8	0.2	0.2
S-5 *Pr* for θ(*η*) profile	1	0.3	0.2	0.2	0.3	**0.1**	0.8	0.2	0.2
	2	0.3	0.2	0.2	0.3	**0.6**	0.8	0.2	0.2
	0	0.3	0.2	0.2	0.3	**1.0**	0.8	0.2	0.2

Table 3: Numerical Parameters of Darcy Forchheimer THNF Flow for Velocity f'(η) and Temperature θ(η).

Scenarios	Cases	Parameters							
		B	*r*	*Fr*	*Ec*	*Pr*	*Sc*	*E*	*k1*
S-6 Sc for φ(η) profile	1	0.1	0.1	0.1	0.1	0.1	**0.1**	0.1	0.01
	2	0.1	0.1	0.1	0.1	0.1	**0.2**	0.1	0.01
	3	0.1	0.1	0.1	0.1	0.1	**0.3**	0.1	0.01
S-7 E for φ (η) profile	1	0.5	0.9	0.3	0.3	1.6	1.3	**0.1**	0.1
	2	0.5	0.9	0.3	0.3	1.6	1.3	**0.6**	0.1
	3	0.5	0.9	0.3	0.3	1.6	1.3	**1.0**	0.1
S-8 k for φ (η) profile	1	0.9	0.2	0.3	0.3	1.6	0.9	0.5	**0.01**
	2	0.9	0.2	0.3	0.3	1.6	0.9	0.5	**0.06**
	3	0.9	0.2	0.3	0.3	1.6	0.9	0.5	**0.10**

Table 4: Numerical Parameters of Darcy Forchheimer THNF Flow for Concentration φ(η).

4. Results and Discussion

This section explores the novel aspects of the key parameters for the flow of the NF ($Mn\ Zn\ Fe_2O_4 + H_2O$) and HNF ($Mn\ Zn\ Fe_2O_4 + Ni\ Zn\ Fe_2O_4 + H_2O$). As such, the features of both the pure and hybrid nanofluids are covered to directly compare the two competitive fluids regarding the impact of the thermophysical parameters on their performances. Finally, we elucidate why HNFs must be preferred over classical NFs. Algebraic setups were used to obtain results by making all the influencers inoperant, leaving only Pr and Sc equal to (0.1). The initiating flow rate, which was based on the equations, is displayed in Table 4. We chose Fr $\leqslant$ 0.3 to avoid a higher nonlinear drag effect and to focus on common and practical scenarios.

Fr	σ_1	σ_2	Python-Generated Velocity f ' (0)
0.1	5%	-	1.4213395
0.2	5%	-	1.3942365
0.3	5%	-	1.3690062
0.1	5%	5%	1.3163499
0.2	5%	5%	1.2912994
0.3	5%	5%	1.2679778

Table 5: Validation of results for initiating velocity with σ_1 and σ_2 as volumetric concentrations of each type of Nano-solute.

Table 5 demonstrate the convergence of the numerical scheme for the velocity at η=0 for two different volumetric concentrations σ_1 and σ_2, of each type of Nano-solute.

Figures 3-5 illustrate the dependence of the velocity f ' (η), temperature θ(η), and concentration profiles (as a function of η) for distinct values of the selected parameters, as listed in Table 3. We validated our results via comparison with the initial velocity (Table 4).

The impact of heat loss due to friction is portrayed in Figure 3(a), which describes the variations in the velocity and inverse Darcy coefficient B of the pure NF and HNF. Increasing the inverse Darcy coefficient B decreased the flow rates. This effect was stronger for the HNF than for the NF. The introduction of a second nanoparticle and increased density caused this decline.

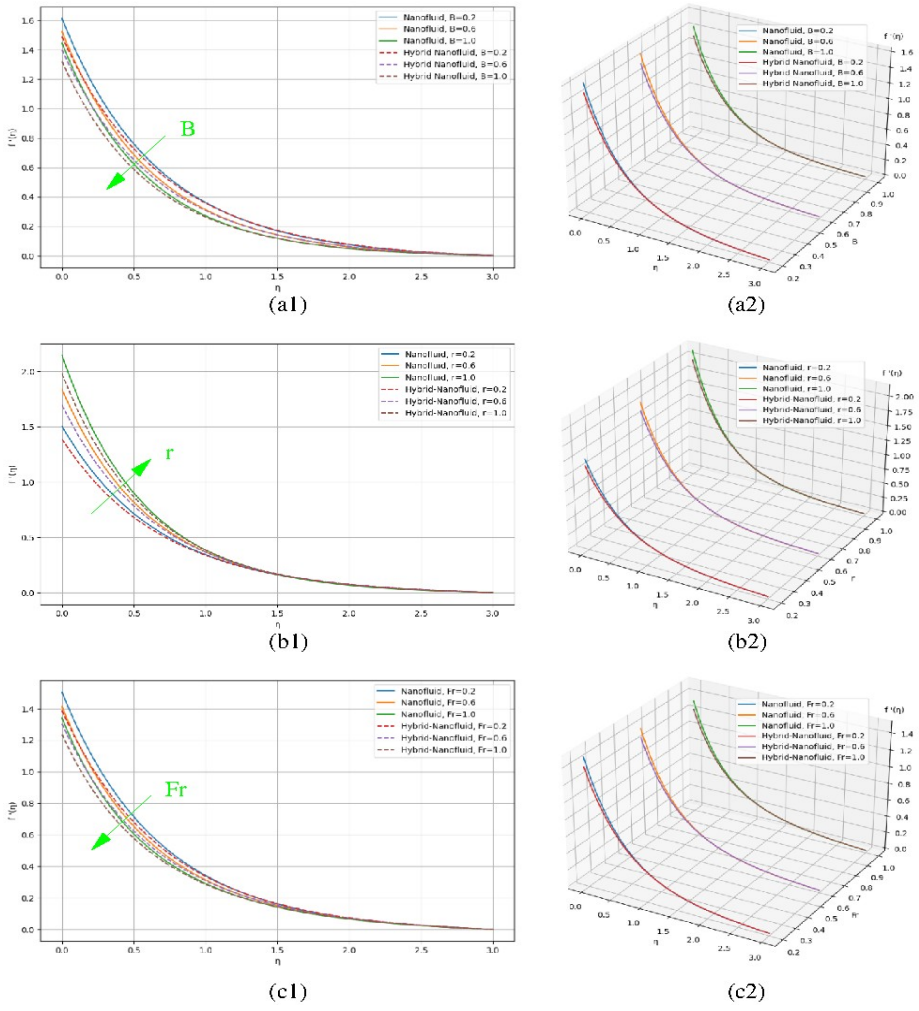

Figure 3: Python-generated velocity f ' (η) profiles of HNF and NF in 2D (1) and 3D (2). Changes in f ' (η) with (a) Inverse Darcy coefficient B, (b) Marangoni coefficient r, and (c) Forchheimer parameter Fr (see Table 3 for further parameters). Arrows in (1) highlight the direction of increase in the corresponding parameter.

Figure 3 (b) shows the inclination in the flow rate by enhancing the Marangoni ratio r. This boost in the flow rate was initially more pronounced in the HNF than in the NF. This resulted from the HNF's enhanced surface tension gradient, thermocapillary effect, and wettability. Boosting the Forchheimer number Fr (Figure 3(c)) resulted in a similar declining trend in the velocity to that observed when increasing B. This declining trend was higher in the HNF than in the NF due to the increased viscidity and volumetric mass. The differences in the velocity profiles f ' (η) between the HNF and NF were largest at small (η) values and decreased with increasing η values as the different curves tended to collapse.

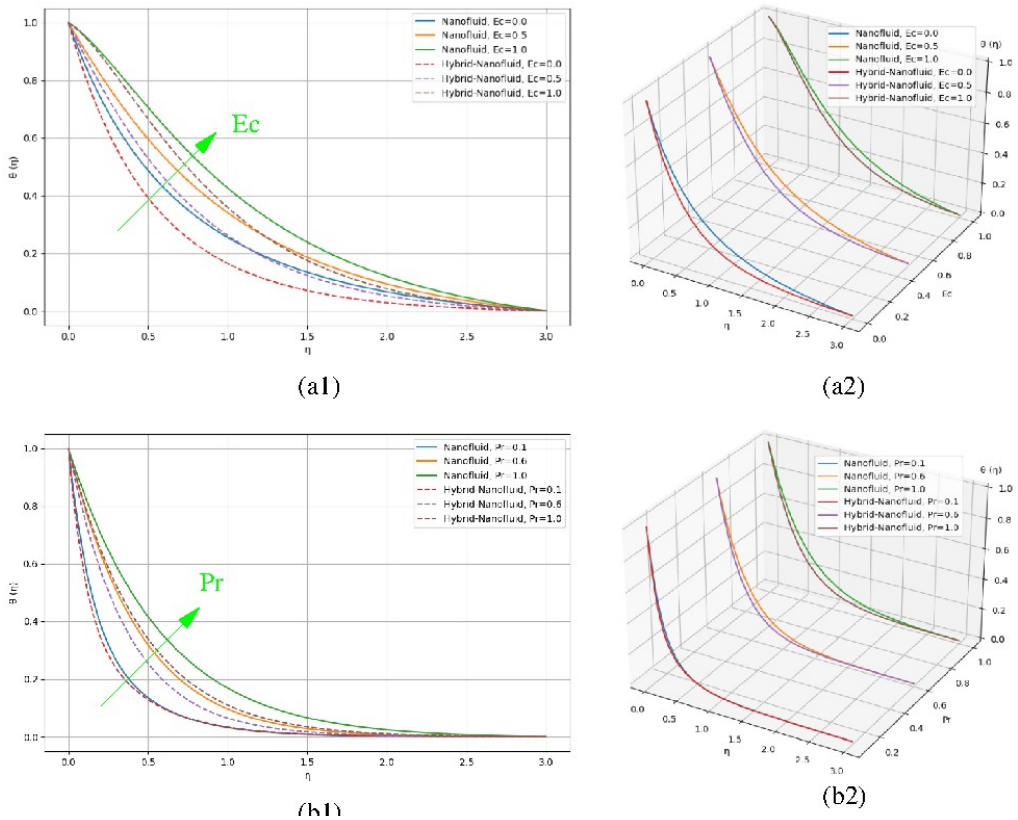

Figure 4: Python-generated temperature profiles θ(η) of HNF and NF in 2D (1) and 3D (2). Changes in θ(η) with (a) Eckert ratio Ec, and (b) Prandtl number Pr (see Table 3 for further parameters). Arrows in (1) highlight the direction of increase in corresponding parameter.

Figure 4 demonstrates the dependence of the temperature profile θ(η) with modifications in the (a) Eckert Ec and (b) Prandtl ratio Pr. We commonly observed that the temperature profiles θ(η) were more strongly affected than the velocity profiles f ' (η) (the curves were more separated). Increasing the Ec or Pr raised the temperature profiles for the HNF and NF similarly. The fluids tended toward reduction in either case (whether pure or hybrid). Meanwhile, qualitatively comparing the curves for the HNF and NF revealed different shapes. The profiles for the HNF were more concave and decreased much faster for small values (η). This was a combined effect of viscous dissipation and reduced thermal transfer. In general, the temperature profile θ(η) significantly differed between the HNF and NF.

We observed an increase in the concentration profile φ (η) (Figure 5) with increasing Schmidt value Sc and activation energy Ec. Conversely, we observed a decline in the concentration with a rise in the chemical reaction rate k1, accounting for species generation/consumption and heat effects. The reaction terms introduced other source terms into the momentum and energy equations, pressure gradients, and temperature distributions, thus affecting the overall flow dynamics. The latter was caused by the larger k1 accelerating the consumption of reactants. Although the HNF and NF exhibited similar differences in the concentration profile φ (η) the curves for the HNF were always above those for the NF.

The HNF's performance for thermo-material transferring applications was always superior to that of the classical NF. The enhanced flow, heat retention, and concentration change of the HNF suggest its potential for enhanced efficiency in thermal management systems, reactors, and other engineering devices where heat and mass transfer are crucial. This detailed insight into the influencing parameters will aid in the development and refinement of advanced thermal management units for diverse industrial applications.

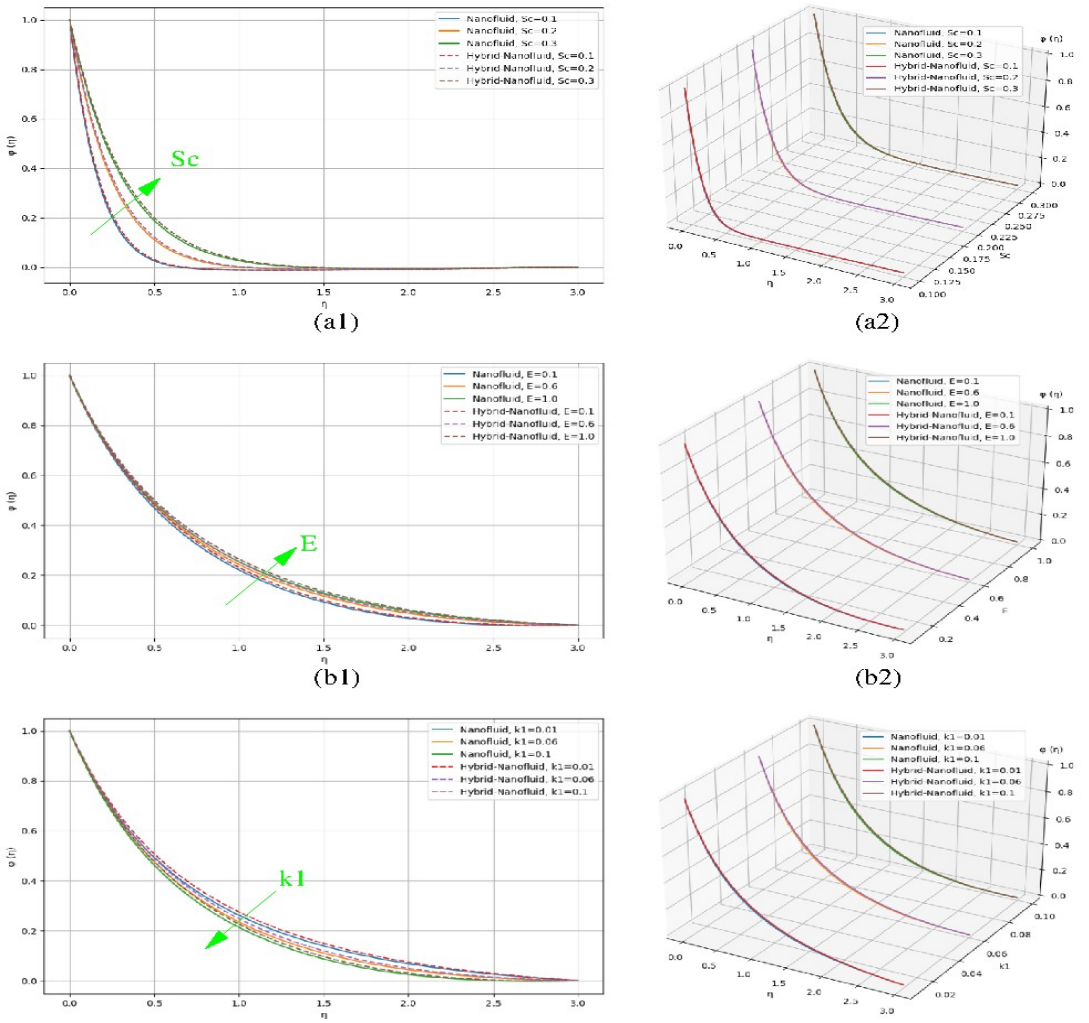

Figure 5: Python-generated concentration profiles φ(η) of HNF and NF in 2D (1) and 3D (2). Changes in φ(η) with (a) Schmidt parameter Sc, (b) Activation energy E, and (c) chemical reaction rate k1 (see Table 4 for further parameters). Arrows in (1) highlight the direction of increase in the corresponding parameter.

The hybrid nanofluid performed better than its classical nanofluid counterpart due to its higher thermal conductivity, which improved its heat transfer efficiency and reduced its thermal resistance, with better control over temperature. The improved flow dynamics were attributed to a decreased effective viscosity, while the enhanced mass transfer rates were due to more pronounced concentration gradients and higher effective diffusivities. The entropy generation analysis showed that viscous dissipation may locally increase due to improved flow, while the enhancement of heat and mass transfer reduces irreversibility's. Interactions with porous media further optimize thermal performance by enhancing heat transfer and changes in the flow patterns, making the HNF highly effective for application in advanced thermal management systems and chemical processing.

5. Conclusions

In this study, we analyzed the Marangoni convective flow through a Darcy–Forchheimer porous matrix using novel theoretical and computational modeling methods for the Marangoni convective flow over a porous surface with a mono nanofluid (NF) and a hybrid nanofluid (HNF) considering modified Darcy–Forchheimer equations. The numerical investigation utilized the modern Python bvp-solver algorithm, which generated optimized outputs. In particular, we investigated the thermal and flow features of the NF ($Mn\ Zn\ Fe_2O_4 + H_2O$) and HNF ($Mn\ Zn\ Fe_2O_4 + Ni\ Zn\ Fe_2O_4 + H_2O$).

This study's results indicate that the flow rate and temperature of HNFs are considerably more pronounced than those of classical NFs. This mainly results from the differences in viscosity and the specific gradient of the surface tension characteristic of HNFs. The prime findings of the problem under consideration are as follows:

• The Marangoni coefficient substantially reduces the velocity f ' (η) for both NFs and HNFs.

• Both the inverse Darcy coefficient and Forchheimer parameter tend to reduce the velocity profile f ' (η)
in NFs and HNFs.

• The temperature is increased with the effects of the Eckert ratio and Prandtl number in usual and hybrid nanofluids.

• The concentration increases due to the effect of the Schmidt parameter and activation energy, whereas it decreases with the chemical reaction rate k1. The effect is similar for NFs and

HNFs.

The main conclusion drawn from this study is that HNFs are generally superior to classical NFs in many ways. HNFs' higher profiles and reaction rates make them highly suitable and favored for thermal control and mass transfer. This is meaningful for future theoretical studies as fundamental research and to improve thermal management in various industrial applications. The presented results will advance the study of Marangoni convective flows in multi-phase, complex porous structures. We hope this research will motivate other researchers to perform additional work in this field

Nomenclature

u, v	Flow rate components	ρ	Density
L*	Diffusion constant	σ 1 , σ2	Volume ratios
T	Temperature	η	Similarity parameter
$c\ p$	Specific thermal capacity	σ0	Surface tension boundary
k	Thermal conductivity	δ 1	Concentration coefficient
r	Marangoni coefficient	Br	Brinkmann number
E	Activation energy	δ	Temperature coefficient
Sc	Schmidt number	k1	Chemical reaction coefficient
Pr	Prandtl ratio	Ec	Eckert number
σ	Surface tension	Fr	Forchheimer number
B	Invers Darcy coefficient	K*	Mass diffusivity
Re	Reynold coefficient	Me	Melting parameter
λ	Porosity parameter	κ	Boltzmann characteristic
HNF	Hybrid nanofluid	NF	Nanofluid

Author Contributions: Conceptualization, H.Q. and S.A.; methodology, H.Q. and S.A.; software, H.Q.; validation, H.Q. and S.A.; formal analysis, H.Q. and S.A.; investigation and data curation, H.Q. and S.A.; writing—original draft preparation and writing—review and editing, H.Q., and S.A.; visualization, H.Q.; supervision, S.A.; project administration, S.A.; All authors have read and agreed to the published version of this manuscript.

Acknowledgments

S. A. is a Serra Húnter Fellow. This work has been supported by the Spanish Government under grant PID2019-105162RB-I00.

Data Availability Statement: The raw data supporting the conclusions of this article will be made available by the authors on request.

Conflicts of Interest: The authors declare no conflicts of interest.

References

1. Liu, S., & Zhu, Q. Y. (2019). Experimental and numerical investigations on combined Buoyancy–Marangoni convection heat and mass transfer of power-law nanofluids in a porous composite with complex surface. *International Journal of Heat and Mass Transfer, 138,* 825-843.
2. Mebarek-Oudina, F. (2019). Convective heat transfer of Titania nanofluids of different base fluids in cylindrical annulus with discrete heat source. *Heat Transfer—Asian Research, 48*(1), 135-147.
3. Mebarek-Oudina, F. (2019). Convective heat transfer of Titania nanofluids of different base fluids in cylindrical annulus with discrete heat source. *Heat Transfer—Asian Research, 48*(1), 135-147.
4. Ahmad Khan, S., & Altamush Siddiqui, M. (2020). Numerical studies on heat and fluid flow of nanofluid in a partially heated vertical annulus. *Heat Transfer, 49*(3), 1458-1490.
5. Reddy, N. K., & Sankar, M. (2020, July). Buoyant convective transport of nanofluids in a non-uniformly heated annulus. In *Journal of Physics: Conference Series* (Vol. 1597, No. 1, p. 012055). IOP Publishing.
6. Sankar, M., Swamy, H. K., Do, Y., & Altmeyer, S. (2022). Thermal effects of nonuniform heating in a nanofluid-filled annulus: Buoyant transport versus entropy generation. *Heat Transfer, 51*(1), 1062-1091.
7. Kashyap, D., & Dass, A. K. (2018). Two-phase lattice Boltzmann simulation of natural convection in a Cu-water nanofluid-filled porous cavity: Effects of thermal boundary conditions on heat transfer and entropy generation. *Advanced Powder Technology, 29*(11), 2707-2724.
8. Chang, J., Nakshatrala, K. B., & Reddy, J. N. (2017).

Modification to Darcy-Forchheimer model due to pressure-dependent viscosity: consequences and numerical solutions. *Journal of Porous Media, 20*(3).
9. Choi, S. U., & Eastman, J. A. (1995). *Enhancing thermal conductivity of fluids with nanoparticles* (No. ANL/MSD/CP-84938; CONF-951135-29). Argonne National Lab. (ANL), Argonne, IL (United States).
10. Buongiorno, J. (2006). Convective transport in nanofluids.
11. Tiwari, R. K., & Das, M. K. (2007). Heat transfer augmentation in a two-sided lid-driven differentially heated square cavity utilizing nanofluids. *International Journal of heat and Mass transfer, 50*(9-10), 2002-2018.
12. Pordanjani, A. H., Aghakhani, S., Afrand, M., Sharifpur, M., Meyer, J. P., Xu, H., ... & Cheraghian, G. (2021). Nanofluids: Physical phenomena, applications in thermal systems and the environment effects-a critical review. *Journal of Cleaner Production, 320,* 128573.
13. Liu, Z., Li, S., Sadaf, T., Khan, S. U., Alzahrani, F., Khan, M. I., & Eldin, S. M. (2023). Numerical bio-convective assessment for rate type nanofluid influenced by Nield thermal constraints and distinct slip features. *Case Studies in Thermal Engineering, 44,* 102821.
14. Soudagar, M. E. M., Shelare, S., Marghade, D., Belkhode, P., Nur-E-Alam, M., Kiong, T. S., ... & Fattah, I. M. R. (2024). Optimizing IC engine efficiency: a comprehensive review on biodiesel, nanofluid, and the role of artificial intelligence and machine learning. *Energy Conversion and Management, 307,* 118337.
15. Wang, X., Song, Y., Li, C., Zhang, Y., Ali, H. M., Sharma, S., ... & Zhou, Z. (2024). Nanofluids application in machining: a comprehensive review. *The International Journal of Advanced Manufacturing Technology, 131*(5), 3113-3164.
16. Sheikholeslami, M., & Khalili, Z. (2024). Simulation for impact of nanofluid spectral splitter on efficiency of concentrated solar photovoltaic thermal system. *Sustainable Cities and Society, 101*, 105139.
17. Bani-Fwaz, M. Z., Mahmood, Z., Bilal, M., Ei-Zahhar, A. A., Khan, I., & Niazai, S. (2024). Computational investigation of thermal process in radiated nanofluid modulation influenced by nanoparticles (Al2O3) and molecular (H2O) diameters. *Journal of Computational Design and Engineering, 11*(2), 22-36.
18. Wang, J., Yang, X., Klemeš, J. J., Tian, K., Ma, T., & Sunden, B. (2023). A review on nanofluid stability: preparation and application. *Renewable and Sustainable Energy Reviews, 188,* 113854.
19. Alsabery, A. I., Abosinnee, A. S., Al-Hadraawy, S. K., Ismael, M. A., Fteiti, M. A., Hashim, I., ... & Chamkha, A. J. (2023). Convection heat transfer in enclosures with inner bodies: A review on single and two-phase nanofluid models. *Renewable and Sustainable Energy Reviews, 183,* 113424.
20. Khan, M., & Khan, W. A. (2016). Steady flow of Burgers' nanofluid over a stretching surface with heat generation/absorption. *Journal of the Brazilian Society of Mechanical Sciences and Engineering, 38*(8), 2359-2367.
21. Modi, K. V., Patel, P. R., & Patel, S. K. (2023). Applicability of mono-nanofluid and hybrid-nanofluid as a technique to improve the performance of solar still: A critical review. *Journal of Cleaner Production, 387,* 135875.
22. Li, S., Puneeth, V., Saeed, A. M., Singhal, A., Al-Yarimi, F. A., Khan, M. I., & Eldin, S. M. (2023). Analysis of the Thomson and Troian velocity slip for the flow of ternary nanofluid past a stretching sheet. *Scientific reports, 13*(1), 2340.
23. Liu, Z., Li, S., Sadaf, T., Khan, S. U., Alzahrani, F., Khan, M. I., & Eldin, S. M. (2023). Numerical bio-convective assessment for rate type nanofluid influenced by Nield thermal constraints and distinct slip features. *Case Studies in Thermal Engineering, 44,* 102821.
24. Chakraborty, S., & Panigrahi, P. K. (2020). Stability of nanofluid: A review. *Applied Thermal Engineering, 174*, 115259.
25. Alsabery, A. I., Abosinnee, A. S., Al-Hadraawy, S. K., Ismael, M. A., Fteiti, M. A., Hashim, I., ... & Chamkha, A. J. (2023). Convection heat transfer in enclosures with inner bodies: A review on single and two-phase nanofluid models. *Renewable and Sustainable Energy Reviews, 183*, 113424.
26. Awan, S. E., Raja, M. A. Z., Mehmood, A., Niazi, S. A., & Siddiqa, S. (2020). Numerical treatments to analyze the nonlinear radiative heat transfer in MHD nanofluid flow with solar energy. *Arabian Journal for Science and Engineering, 45,* 4975-4994.
27. Li, Y. X., Mishra, S. R., Pattnaik, P. K., Baag, S., Li, Y. M., Khan, M. I., ... & Khan, S. U. (2022). Numerical treatment of time dependent magnetohydrodynamic nanofluid flow of mass and heat transport subject to chemical reaction and heat source. *Alexandria Engineering Journal, 61*(3), 2484-2491.
28. Ellahi, R., Tariq, M. H., Hassan, M., & Vafai, K. (2017). On boundary layer nano-ferroliquid flow under the influence of low oscillating stretchable rotating disk. *Journal of Molecular Liquids, 229,* 339-345.
29. Muneeshwaran, M., Srinivasan, G., Muthukumar, P., & Wang, C. C. (2021). Role of hybrid-nanofluid in heat transfer enhancement–A review. *International Communications in Heat and Mass Transfer, 125,* 105341.
30. Sarkar, J., Ghosh, P., & Adil, A. (2015). A review on hybrid nanofluids: recent research, development and applications. *Renewable and Sustainable Energy Reviews, 43,* 164-177..
31. Qureshi, M. A. (2022). Thermal capability and entropy optimization for Prandtl-Eyring hybrid nanofluid flow in solar aircraft implementation. *Alexandria Engineering Journal, 61*(7), 5295-5307.
32. Jamshed, W., Safdar, R., Brahmia, A., Alanazi, A. K., Abo-Dief, H. M., & Eid, M. R. (2023). Numerical simulations of environmental energy features in solar pump application by using hybrid nanofluid flow: Prandtl-Eyring case. *Energy & Environment, 34*(4), 780-807.
33. Shah, Z., Rooman, M., & Shutaywi, M. (2023). Computational analysis of radiative engine oil-based Prandtl–Eyring hybrid nanofluid flow with variable heat transfer using the Cattaneo–Christov heat flux model. *RSC advances, 13*(6), 3552-3560.
34. Shehzad, S. A., Sheikholeslami, M., Ambreen, T., & Shafee, A. (2020). Convective MHD flow of hybrid-nanofluid within an elliptic porous enclosure. *Physics Letters A, 384*(28), 126727.
35. Radhika, M., Punith Gowda, R. J., Naveenkumar, R.,

Siddabasappa, & Prasannakumara, B. C. (2021). Heat transfer in dusty fluid with suspended hybrid nanoparticles over a melting surface. *Heat Transfer, 50*(3), 2150-2167.
36. Ahmad, B., Abbas, T., Fatima, K., Duraihem, F. Z., & Saleem, S. (2024). Nonlinear flow of hybrid nanofluid with thermal radiation: A numerical investigation. *ZAMM-Journal of Applied Mathematics and Mechanics/Zeitschrift für Angewandte Mathematik und Mechanik, 104*(1), e202200170.
37. Alqahtani, A. M., Bilal, M., Ali, A., Alsenani, T. R., & Eldin, S. M. (2023). Numerical solution of an electrically conducting spinning flow of hybrid nanofluid comprised of silver and gold nanoparticles across two parallel surfaces. *Scientific Reports, 13*(1), 7180.
38. Ali, B., Mishra, N. K., Rafique, K., Jubair, S., Mahmood, Z., & Eldin, S. M. (2023). Mixed convective flow of hybrid nanofluid over a heated stretching disk with zero-mass flux using the modified Buongiorno model. *Alexandria Engineering Journal, 72,* 83-96.
39. Hussain, M., Imran, M., Waqas, H., Muhammad, T., & Eldin, S. M. (2023). An efficient heat transfer analysis of MHD flow of hybrid nanofluid between two vertically rotating plates using Keller box scheme. *Case Studies in Thermal Engineering, 49,* 103231.
40. Lund, L. A., Yashkun, U., & Shah, N. A. (2023). Magnetohydrodynamics streamwise and cross flow of hybrid nanofluid along the viscous dissipation effect: Duality and stability. *Physics of Fluids, 35*(2).
41. Qureshi, H., Shah, Z., Raja, M. A. Z., Shoaib, M., & Khan, W. A. (2024). Machine learning investigation for tri-magnetized Sutterby nanofluidic model with Joule heating in agrivoltaics technology. *NANO*.
42. Qureshi, H., Pasha, A. A., Shah, Z., Raja, M. A. Z., Algarni, S., Alqahtani, T., ... & Khan, W. A. (2024). Application of machine learning for thermal exchange of dissipative ternary nanofluid over a stretchable Wavy cylinder with thermal slip. Case Studies in Thermal Engineering, 104599.
43. Qureshi, H., Shah, Z., Raja, M. A. Z., Shoaib, M., & Khan, W. A. (2024). Supervised machine learning computing paradigm to measure melting and dissipative effects in entropy induced Darcy–Forchheimer flow with ternary-hybrid nanofluids. *Numerical Heat Transfer, Part B: Fundamentals,* 1-22.
44. Khan, M. I., Qayyum, S., Shah, F., Kumar, R. N., Gowda, R. P., Prasannakumara, B. C., ... & Kadry, S. (2021). Marangoni convective flow of hybrid nanofluid (MnZnFe2O4-NiZnFe2O4-H2O) with Darcy Forchheimer medium. *Ain Shams Engineering Journal, 12*(4), 3931-3938.
45. Abrar, M. N. (2024). Entropy analysis of double diffusion in a Darcy medium with tangent hyperbolic fluid and slip factors over a stretching sheet: Role of viscous dissipation. *Numerical Heat Transfer, Part A: Applications,* 1-14.
46. Berg, J. C., Mahr, T. G. (2015). Marangoni convection. Annual Review of Fluid Mechanics, 47, 141-165.
47. Darcy, H. (1856). Les fontaines publiques de la ville de Dijon. Victor Dalmont.
48. Forchheimer, P. (1901). Wasserbewegung durch Boden. Zeitschrift des Vereines deutscher Ingenieure, 45(45), 1782-1788.
49. Reynolds, O. (1883). III. An experimental investigation of the circumstances which determine whether the motion of water shall be direct or sinuous, and of the law of resistance in parallel channels. *Proceedings of the royal society of London, 35*(224-226), 84-99.
50. Prandtl, L. (1904). Über Flüssigkeitsbewegung bei sehr kleiner Reibung, Verhandlungen des dritten internationalen Mathematiker-Kongresses.
51. Nusselt, W. (1915). Die Abhängigkeit der Wärmeübertragung von der Rohrlänge. *Zeitschrift des Vereines deutscher Ingenieure, 59*(11), 541-546.